Dividing Blobs, Chemical Flowers, and Patterned Islands in a Reaction−Diffusion System

P. W. Davies, P. Blanchedeau, E. Dulos, and P. De Kepper*

Centre de Recherche Paul Pascal/CNRS, Université Bordeaux I, Avenue A. Schweitzer, F-33600 Pessac, France

Received: April 28, 1998; In Final Form: July 31, 1998

In an one-side-fed open spatial reactor operated with the chlorine dioxide−iodine−malonic acid reaction in the presence of polyvinyl alcohol, we systematically studied the growth dynamics of Turing patterns after a supercritical parameter change. We describe different modes of propagation of the patterned state in an absolutely unstable uniform state, among which are a spot division and a finger splitting mode. We attribute these peculiar growth modes to the existence of two different uniform states and to a morphological instability of a propagating front linking these two states. In regions where bistability between the Turing state and a uniform state is obtained, the interface between the patterned state and the uniform state can be brought to a halt and thus localized patterned states are observed.

1. Introduction

Far from thermodynamic equilibrium, chemical reactions with appropriate feedback mechanisms can develop traveling and stationary patterns of chemical activity. Of particular interest to us is the spontaneous development of stationary patterns resulting from the sole interaction between local chemical processes and the diffusive transport of solvated species. Such patterns were predicted by Turing in 1952,[1] nearly 40 years before their first unambiguous observation in a single-phase reacting system.[2] The discovery is associated with the development of open spatial reactors.[2−6] It induced a renewal of experimental and theoretical studies of chemical patterns. Today, there is not only a large number of works on Turing instability[6] and its interaction with the oscillatory Hopf instability,[6−9] but also on the more recently observed morphological instability of traveling fronts in bistable systems[10,11] All of these new studies broaden the scope of chemical patterns substantially beyond that of excitation waves, the study of which began in the early 1970s.[12,13] Much of the interest in chemical patterns and waves stems from some striking similarities with pattern development in living systems and from the fact that reaction−diffusion mechanisms are often evoked in biological morphogenesis.[1,14−18] In some respects, chemical reaction−diffusion systems can be thought as experimental toy models for a number of biological phenomena.

For stationary Turing patterns, previous studies essentially focused on the properties of the asymptotic states of the system and little attention was directed to the growth dynamics of these patterns. In contrast, this report focuses on the growth dynamics of Turing patterns out of a uniform state, more precisely on the stability and dynamics of the interface between the Turing state and the uniform state.

Most preceding works on Turing patterns were performed in open spatial reactors made of a relatively thick disk of gel, fed from opposing circular faces with different subsets of chemicals. The standard two-dimnensional (2-D) asymptotic patterns, consisting of hexagonal arrays or periodic parallel lines of stationary concentration extrema, were readily observed in these reactors[6,8,19,20] when operated with the original chlorite−iodide−malonic acid (CIMA) reaction[21] and its central variant, the chlorine dioxide−iodine−malonic acid (CDIMA) reaction.[22] More exotic stationary patterns have also been observed in these reactors but the status of these nonstandard planforms is not always clear. They are interpreted either as resonant harmonic patterns developing far from onset,[23,24] as the result of new stable symmetries due to strong parameter gradients, or as mere moiré effects resulting from unresolved three-dimensional (3-D) structures.[25,26]

Although the two-side-fed spatial reactors have some advantages (i.e., the reaction essentially operates inside the gel medium at a distance from the boundaries), they also have the drawback of introducing steep concentration gradients of principal reagents. The concentration profiles of the feed species cannot be directly controlled and the patterns are confined inside a more or less thick stratum of unknown chemical composition between the feed surfaces. Furthermore, this composition varies in the thickness and consequently, different types of patterns or classes of instabilities can develop at different adjacent positions and interact.[8,26] These drawbacks make interpretation difficult in the present state of theory development.

To avoid these complications, we have used another reactor geometry: It consists of a thin disk of gel in contact only by one face with the contents of a continuously fed strirred tank reactor (CSTR). If the thickness of the gel medium is equal to or smaller than the wavelength of the patterns and corresponds to a diffusion time of the order or less than the reaction time, this open spatial reactor can approximate a 2-D reaction−diffusion system with uniform constraints. It has been shown that this is the case when the CDIMA reaction is operated in such a one-side-fed spatial reactor. Different sections of the phase diagram of this reaction−diffusion system were established as a function of the feed concentrations of chlorine dioxide (ClO_2) and malonic acid (MA), two initial reagents, and of polyvinyl alcohol (PVA), a polymer which serves both as a color indicator for the reaction and as a species controlling the effective diffusion of the main activatory species of the reaction. The experimental phase diagram of patterns in the

* To whom correspondence should be addressed. E-mail: dekepper@crpp.u-bordeaux.fr.

10.1021/jp982034n CCC: $15.00
Published on Web 10/01/1998

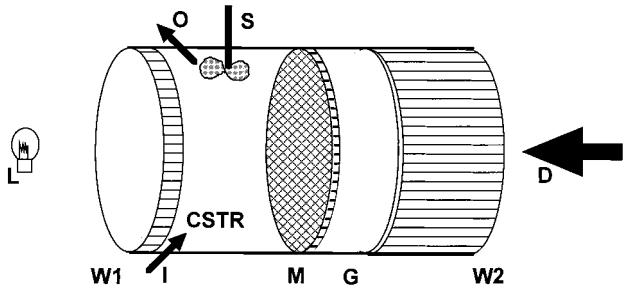

Figure 1. Schematic representation of the one-side-fed disk reactor. W1: white window, W2: transparent window, L: light source, M: capillary Anotec membrane, G: disk of agarose gel, D: direction of observation, I and O: inlets and outlet, respectively, of the CSTR, S: stirrer.

disk of gel can be nearly quantitatively accounted for by a 2-D version of a skeleton kinetic model of the CDIMA reaction proposed by Lengyel and Epstein.[27] Detailed bifurcation diagrams and comparisons with kinetic model predictions can be found elsewhere.[28−30] However, one has to be aware that dynamic instabilities such as oscillations and multistabilities can develop in the CSTR, because the full reaction already proceeds there. Such instabilities could lead to very complex pattern dynamics in the gel. In the present work, such regions of the phase diagram are avoided.

2. Experimental Conditions

Apparatus, Reagents, and Procedure. A sketch of the one-side-fed reactor appears in Figure 1. The CSTR is permanently fed with three separated solutions of the initial reagents of the CDIMA reaction, prepared in three separated reservoirs. The solutions are made with high-quality deionized water (Milli-Q, Millipore) and each contains 1×10^{-2} M of sulfuric acid (H_2SO_4). One reservoir contains a saturated solution (at room temperature) of iodine (I_2 from Vorsicht, Suptapur). A second reservoir contains variable concentrations of MA ($CH_2(COOH)_2$ from Fluka, puriss.) and PVA ((($-CH_2CHOH-)_x$, ($-CH_2CH(O_2CCH_3-)_y$) from Aldrich, 80% hydrolyzed, MW $\simeq$ 10 000). The third reservoir contains a solution of ClO_2[31] refrigerated at 0 °C. Equal flows of these solutions (36 cm^3/h) were pumped (P500 pumps from Pharmacia) and premixed just before being injected into the CSTR. The same residence time of the stirred reactor, $\tau = 8$ min, was maintained during all of the experiments. The whole reactor system is immersed into a thermostated bath at $T = 5$ °C. At room temperature, iodine has a high vapor tension and chlorine dioxide is a gas. Consequently, these species can diffuse across the walls of the polytetrafluoroethylene (PTFE) tubings inside which they are conveyed from the reservoirs to the reactor. The losses were measured and the constraint values reported are corrected for these losses. The qualitative changes of state of the contents of the CSTR were monitored with a Pt electrode. No attempt was made to connect this electropotential measurement to quantitative concentration changes.[32] The disk of hydrogel, 0.2 mm thick, was made of 2% agarose (Fluka 0570) loaded with the same concentration of PVA as the mix in the CSTR. One face of the disk was in contact with the contents of the CSTR, the other face was pressed against an impermeable surface. To provide rigidity to the soft disk of hydrogel, a very thin mineral membrane (Anotec from Whatman, 0.06 mm thick with unidirectional pores of 0.02 μm) was interposed between the gel and the solution in the CSTR. This membrane also prevented the hydrodynamic turbulence from disturbing the patterns that could spread up to the surface of the gel. Furthermore, it provided an effective decoupling between the variables in the CSTR and in the gel, a fundamental requirement for any spontaneous spatial instability to develop in the gel.[6] During all of these experiments $[I_2]_0$ was fixed at 3.34×10^{-4} M.

When a supercritical change of parameter is made from a region of uniform steady state into the Turing state domain, the patterned state usually starts to develop from the rim of the disk or from more or less numerous random locations in the gel. These locations sometimes correspond to visible dust particles. To gain some control on the position where the pattern would first nucleate and to be able to clearly observe fronts between different states, we introduced in the center of the disk of gel a tiny silver particle which acted as a suitable punctual nucleation site for the development of patterns. The typical size of this silver particle was 0.05 mm. In other cases, we isolated part of the disk from the contents of the CSTR with a rectangular impermeable mask, an edge of which acted as a linear initiator of the patterned state. The latter technique will not be illustrated in this report because it essentially shows the same type of pattern growth as that obtained with a punctual initiator.

3. Experimental Results

Before presenting our results on pattern growth dynamics, we will discuss the role of a number of species, in particular that of PVA. The CDIMA reaction is an oscillatory redox reaction, the kinetic mechanism of which has been elucidated.[33] In first approximation, the oscillatory behavior and the patterning processes are controlled by the iodide and chlorite concentrations. These two intermediate species act respectively as the main activatory and inhibitory species of the reaction. When a reaction system can be described by a two-variable kinetic model, it can give rise to Turing patterns only if the effective diffusion coefficient of the activatory species is sufficiently less than that of the inhibitory species. PVA, the macromolecule that selectively and reversibly binds iodide, in the presence of iodine, is the only species with reduced mobility in the gel. As a result, the effective diffusivity of iodide, the activator, is reduced.[28,34] It is shown theoretically and experimentally that, if the PVA complex with the activator is nonreactive, this complexing agent also acts as a buffer for the activator and can stabilize the steady states at the expense of the oscillatory state. This is illustrated in Figure 2, in which are plotted the electrochemical potential of the solution in the CSTR as a function of $[MA]_0$, both in the absence and in the presence of PVA. The figure shows that, at low $[MA]_0$ and in the absence of PVA, the reaction mixture exhibits a high potential steady state. When $[MA]_0$ exceeds 1.5×10^{-4} M, small amplitude potential oscillations are detected. The amplitude of these oscillations first grows with increasing $[MA]_0$ and becomes as large as 200 mV, then it starts to decrease and suddenly oscillations give place to a new steady state with low potential values. Note the large potential difference between the two steady states. In the presence of 10 g/L of PVA, oscillations are completely suppressed over the same range of $[MA]_0$ and only a smooth change of the steady state potential is measured. In fact, as $[PVA]_0$ is gradually increased, the extent of the domain of oscillations as a function of $[MA]_0$ shrinks and finally vanishes at a critical $[PVA]_0$. This critical value decreases with decreasing values of $[ClO_2]_0$. For $[ClO_2]_0 = 2 \times 10^{-4}$ M, which corresponds to the case in Figure 2, the critical value is about 2.25 g/L. The experiments reported in this paper correspond to conditions in which any oscillatory behavior has disappeared, in the CSTR, as a function of $[MA]_0$. In these conditions, two

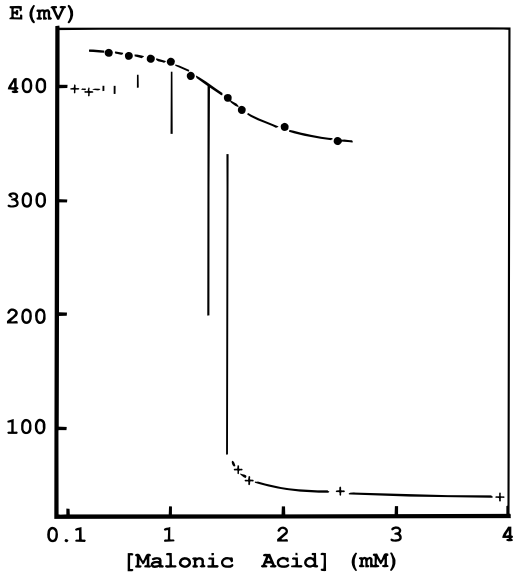

Figure 2. Dynamics of the CSTR. Potential E of an uncalibrated Pt electrode versus $Hg/Hg_2SO_4/K_2SO_4$ reference electrode. Stationary states: (+) in the absence of PVA, (●) in the presence of 10 g/L of PVA. The vertical lines correspond to the amplitude of oscillatory states.

different uniform steady states may be distinguished in the gel: one of them (USS1), characterized by a dark purple or reddish-purple color, is observed at low MA feed concentration, and the other (USS2), observed at high MA feed concentration, is characterized by a pale purple or pinkish color. Between these two uniform states, a domain of Turing pattern displays the usual 2-D hexagon or stripe planforms.

We now describe the growth dynamics of Turing patterns as a supercritical change in control parameter is made that drives the system from the USS1 domain to the Turing region and beyond. The control parameter used in this series of experiments is the feed of MA.

Growth Dynamics. At high ClO_2 feed concentration or at low $[PVA]_0$, starting from USS1, a change of $[MA]_0$ just beyond onset brings up a more or less random development of spots that ultimately organize in clusters of regular hexagonal arrays. This is the most usual growth mode for Turing patterns both in experiments and in numerical simulations close to onset. We refer to it as the standard growth mode. In these regions of feed concentration, it was difficult to produce a long lasting neat interface between the growing Turing mode and the initial uniform state.

At low $[ClO_2]_0$ or high enough PVA concentration, new types of pattern growth dynamics are readily observed. A typical sequence of states, as a function of MA, is reported in Figure 3. No hysteresis within the accuracy of 2% on parameter values was observed at the transition between the uniform states and the Turing pattern states. We now describe the growth dynamics of the Turing patterns as different supercritical changes in control parameter are made from USS1 into the Turing region and beyond. The initial feed composition is always the same. Starting from this composition, other different compositions are reached in a single step and correspond to the $[MA]_0$ jumps "1,2,3,4" in Figure 3. In all cases, after the supercritical change of $[MA]_0$, a clear spot (low iodide region) develops around the silver particle. As it will be shown in the following discussion, the fate of this growing spot depends on the new feed composition.

Dividing Blobs. When the change is made to compositions just beyond the Turing bifurcation line (e.g., jump 1 in Figure

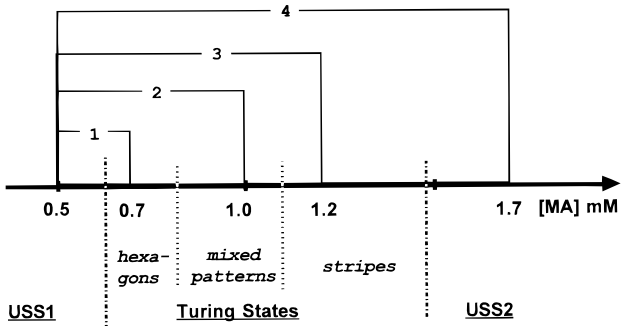

Figure 3. State diagram as a function of malonic acid and schematic representation of the experimental procedure. Other constraints: $[ClO_2]_0 = 2 \times 10^{-4}$ M, $[PVA]_0 = 10$ g/L, $[H_2SO_4]_0 = 1 \times 10^{-2}$ M, $T = 5$ °C, $\tau = 8$ min.

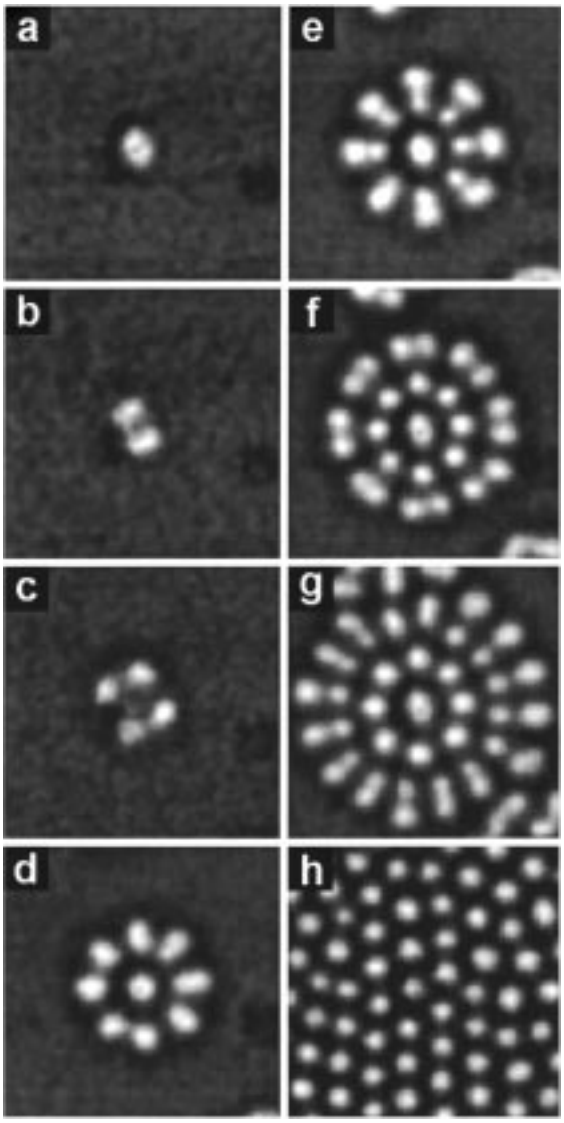

Figure 4. Dividing blobs. Series of photographs corresponding to a pattern growth after jump 1 in Figure 3: photographs (a−g) taken at 45-min intervals, (h) taken 14 h after the concentration change.

3), the initial clear spot slowly swells then divides into two equal daughter spots, which in turn, swell and divide (Figure 4). At least up to the stage of 16 peripheral spots, the division mechanism proceeds alternatively in the azimuthal and radial directions in order to fill the growing interface between the uniform state USS1 and the patterned cluster. Spots inhibit the formation of new daughters in their immediate proximity so that

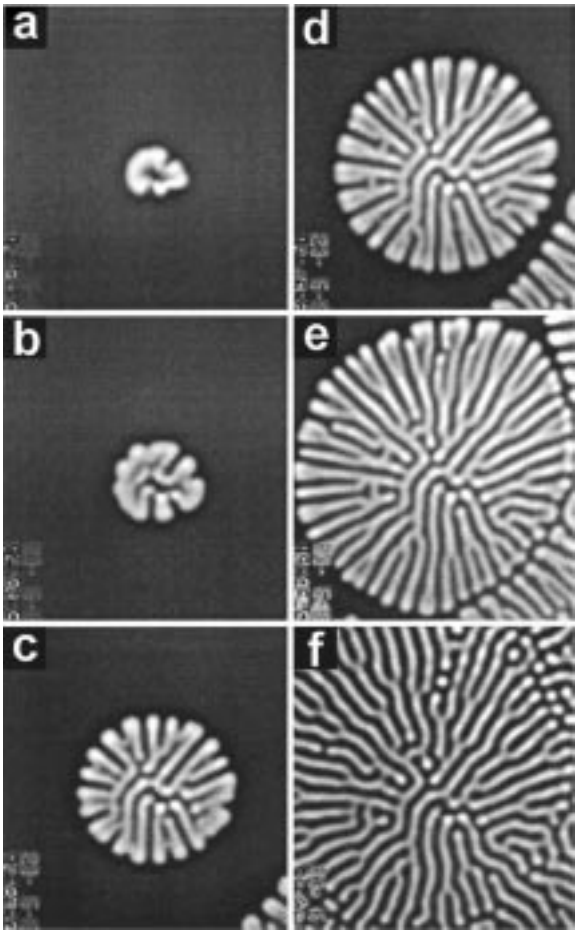

Figure 5. Flower-like pattern. Pattern growth after jump 3 in Figure 3. Photographs taken (a) 12 min, (b) 20 min, (c) 35 min, (d) 52 min, (e) 75 min, and (f) 7 h after the initial growth of the pattern.

the division mechanism essentially proceeds at the interface with the USS1 state. In the initial stages, the spot arrangement in the cluster is more "square-like" than hexagonal, but the pattern extrema very slowly rearrange to produce more regular domains of hexagonal patterns (Figure 4h). The average radial expansion rate of the cluster is very slow close to onset, about 0.6 mm/h. One full cell division takes about 30 min.

Chemical Flowers. If the parameter jump brings the system to a composition close to the high malonic acid concentration end of the Turing domain (e.g., jump 3 in Figure 3), another unusual pattern growth mechanism is observed (Figure 5). The small clear spot around the silver particle initially grows as a smooth clear disk, the center of which gradually returns to a darker level of grey. Then, we are left for a time with a clear ring. When this ring reaches a diameter of about 1.5 mm, the interface with USS1 starts to undulate (Figure 5a). The undulations then develop into clear fingers which extend radially. After a while, each fingertip divides in two daughter fingers which in turn divide as the tips run away from the center. The overall mechanism produces flower-like patterns. The combination of tip division and finger splitting mechanisms is clearly demonstrated in Figure 6, in which binarized images of the pattern at different stages of development were additively superimposed. Ultimately, a standard striped Turing pattern is obtained (Figure 5f). Fingers grow radially but stripes slowly rearrange in parallel by drifts and reconnections. The average radial expansion rate of this flower-like pattern is 3.3 mm/h, five times faster than for the dividing spots. This is all natural,

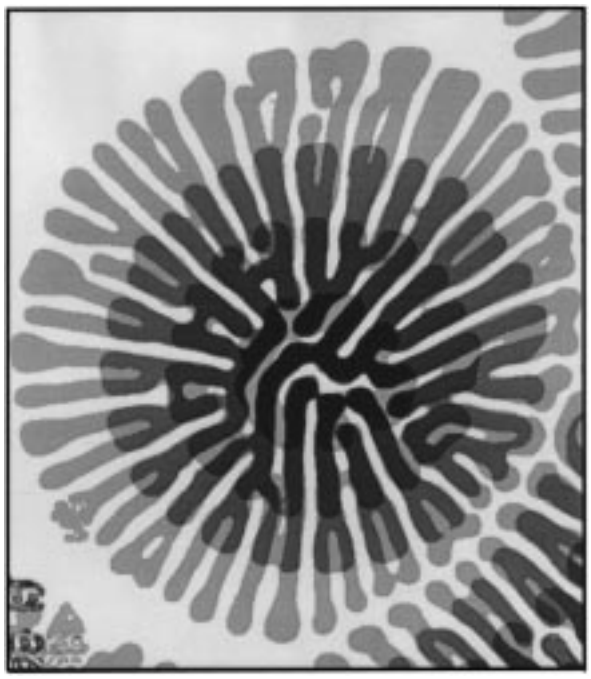

Figure 6. Finger splitting mechanism. Additive superposition of binarized images of the sequence in Figure 5.

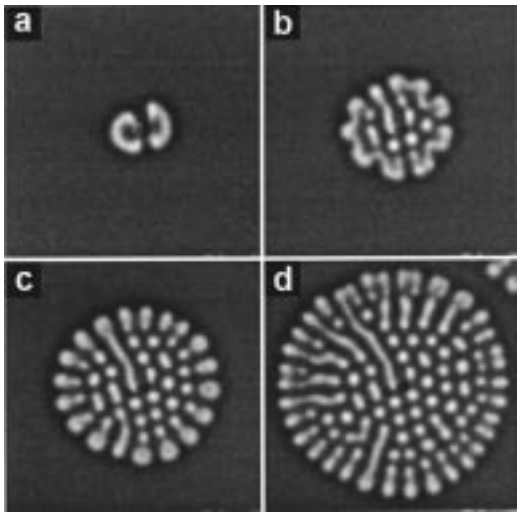

Figure 7. Flower-like pattern. Pattern growth after jump 2 in Figure 3. Photographs taken (a) 16 min, (b) 55 min, (c) 2 h, 35 min, and (d) 3 h, 25 min after the initial growth of the pattern.

because the jump is made deep inside the Turing domain to a composition for which the initial uniform state is much more unstable.

For concentration jumps between the two above-described limit cases, many intermediate situations are observed. If the composition change drives the system in the mixed pattern region (e.g., jump 2 in Figure 3), the growing flower-like pattern propagates as small fingers (Figure 7) which soon break down into spots at a more or less short distance from the interface with the uniform state.

We have extended the study to parameter jumps beyond the Turing pattern domain, to values corresponding to the other uniform state USS2 (e.g., jump 4 in Figure 3). In these cases, composed flower-like patterns temporarily develop, fill all the space, and eventually vanish. A time sequence of this case is illustrated in Figure 8. Three different states can temporarily coexist: the initial USS1 (dark uniform state), the patterned Turing state, and USS2 (clear uniform state). Remarkably,

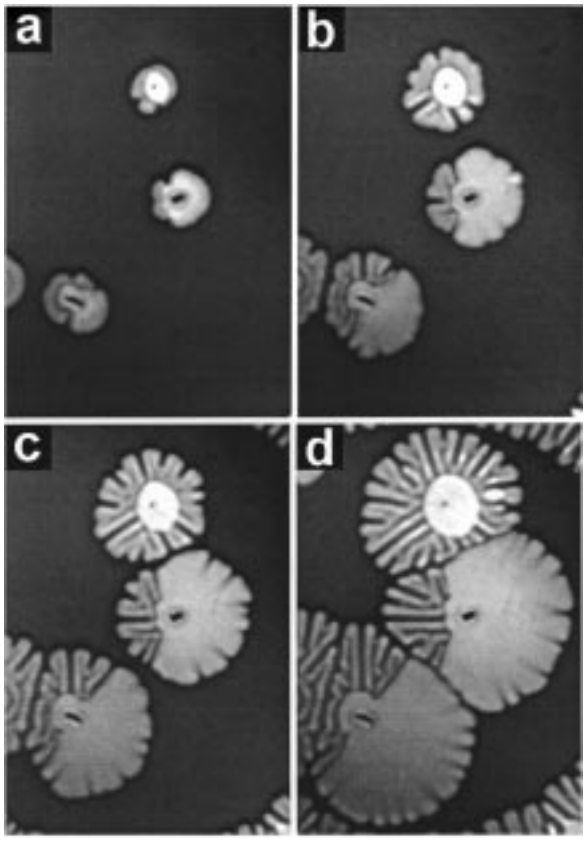

Figure 8. Flower-like pattern. Series of photographs corresponding to a pattern growth after jump 4 in Figure 3. Pictures taken (a) 8 min, (b) 18 min, (c) 33 min, and (d) 53 min after the initial growth of the pattern.

TABLE 1: Growth Rates of Flower-like Patterns as a Function of Different Composition Jumps

$[MA]_0$ (mM)	$\Delta r/\Delta t$ (mm/h)	λ (mm)
0.5	initial USS1	
0.69	0.6	0.43
0.76	1.0	0.47
1.2	3.3	0.46
1.52	3.2	
1.7	3.9	

"interfaces" between any of these three states may simultaneously be observed. In particular, a direct transition between the two uniform states is witnessed. This interface or front is not monotonically curved but exhibits indentations with a wavelength about twice that of the neighboring Turing patterns. The radial expansion rate of these new flower patterns is relatively fast. Of course, in this domain of feed concentration, the Turing patterns are transient and the system will end up in the second uniform state. The growth rates of the flower-like patterns as a function of different composition jumps are listed in Table 1. Note also that the wavelength of the asymptotic Turing patterns depends only very slightly on the MA feed concentration.

Occasionally, in the first stages of development of the flower patterns, the initial clear spot forms a thick clear ring, which as it spreads, splits once or twice and drops back circular stationary stripes. These sooner or later break and recombine to provide the usual more or less twisted parallel stripe pattern. The photographs (Figures 9a−c) provide a global view of the growing 2-D pattern at three different times. A plot of the light intensity as a function of time, along a line passing by the middle of the initial spot (Figure 9d), demonstrates this ring splitting

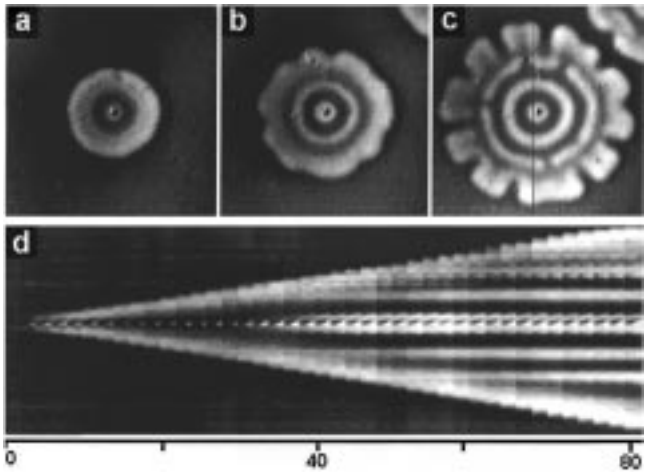

Figure 9. Splitting ring. Same conditions as in Figure 5. Photographs taken (a) 36 min, (b) 52 min, and (c) 72 min after the MA feed concentration change. (d) Space−time plot of the light intensity along the dark line in photograph (c).

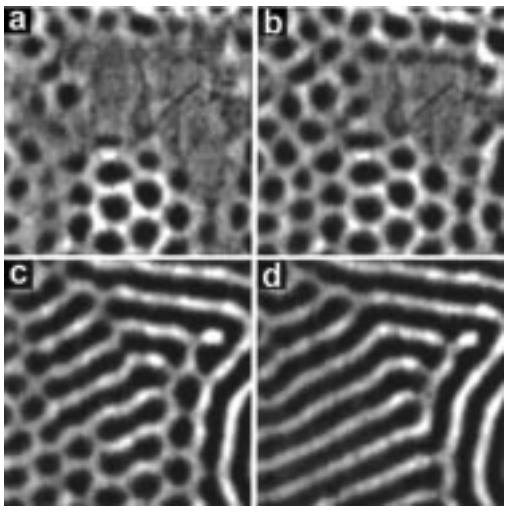

Figure 10. Growth dynamics of a transient dark spot pattern, obtained by decreasing in one step the malonic acid feed concentration from 1.7×10^{-3} M to 1.5×10^{-3} M. Intervals between photographs are 12 min, 60 min, and 120 min, respectively.

phenomenon. Figure 9d shows that the external front propagates at constant velocity, as long as it does not meet another front. At about 36 min after the concentration jump, a first clear circular stripe separates from the expanding annulus and remains stationary. Although the front of the propagating ring starts to show protrusions, the back of the wave is still quite smooth and a second clear stripe comes off a little later. This second circular stripe has a greater proclivity to break and reconnect.

Transient Dark Spot Pattern. In addition, we explored the pattern growth dynamics when, starting from the USS2, the MA feed concentration was decreased. In most cases, a supercritical parameter change produced a random growth of clear spots which asymptotically rearranged in more regular stripe or hexagonal array of clear spots according to the new feed composition. However, if the change was made just beyond onset, strangely, clusters of dark spot patterns first slowly grew in the clearer USS2 state. An interface between this new Turing pattern and USS2 can be obtained. As shown in Figure 10, spots gradually emerge at the interface in staggered position with the dark spikes in the patterned area. This inversed color dappling pattern was transient. Eventually, spots slowly connected to produce the usual stripe pattern found in this region

TABLE 2: Hysteresis Cycle between an Hexagonal Turing State and the USS1 State

response	$[ClO_2]_0$ (mM)					
	0.2	0.078	0.066	0.06	0.044	0.033
state	hex →	hex →	hex →	hex →	hex →	USS1
state		hex ←	USS1 ←	USS1 ←	USS1 ←	USS1
λ (mm)	0.4	0.5	0.6	0.71	0.89	

of the phase diagram. It is noteworthy that we were never able to find a composition in which this hexagonal array of dark spot pattern could be stabilized. However, its lifetime seemed to increase with increasing concentration of PVA. On the basis of theoretical calculations on a skeleton model of the CDIMA reaction, stable dark hexagons are predicted, but at high feed concentration of chlorine dioxide and in the vicinity of USS1.[29,30] This is not at all the region of phase diagram where the present observations were made. Actually, the experimentally observed transition between the Turing state and USS2 was not accounted for by the simple Lengyel−Epstein kinetic model.[30] It is interesting to note that transient hexagonal arrays of dark spots had already been observed in the CIMA reaction in quite different conditions.[6,24,25] However, these earlier observations cannot be compared with either the present experimental observations or with calculations because in earlier experiments, the actual concentrations of major reagents in the gel were unknown.

Localized Patterns. In the above-described set of experiments, only propagating fronts between two states were obtained. In particular, the fronts between the spotted Turing state and the uniform states could not be brought to a halt without leading to the recession of the Turing state. Theoretical studies predict the possibility of immobilizing the interface between an hexagonal Turing state and the uniform state in subcritical regions of the Turing bifurcation.[35] Such a front-pinning phenomenon can be due to nonadiabatic[36] and/or nonpotential[37] effects, in regions of control parameter exhibiting multistability between states. The above experimental observations are consistent with the fact that within our experimental accuracy, no hysteresis between the Turing state and the uniform states was observed. Although theoretical analysis tells us that the bifurcation from uniform state to hexagonal structures is generally subcritical, this region of subcriticallity seems to be very reduced as a function of $[MA]_0$, under the experimental conditions selected above.

However, a large region of hyteresis between the Turing state and a dark uniform state is found (Table 2), if for appropriate fixed $[MA]_0$, $[ClO_2]_0$ is decreased. Within this region of hysteresis, different localized stable clusters of Turing state (containing one to a few spots) could be embedded in the uniform state. An experiment leading to such an isolated patterned island is described below and is illustrated by the sequence of photographs in Figure 11. Much like in the previous experiments, we start from the uniform state and the growth of a flower-like pattern is initiated by feeding the reactor with $[ClO_2]_0 = 2 \times 10^{-4}$ M and $[MA]_0 = 7.8 \times 10^{-3}$ M. In these new experiments, all other parameters are set as above except $[PVA]_0 = 4.5$ g/L. When the flower pattern is sufficiently developed (Figure 11a), the feed concentration of ClO_2 is suddenly decreased to 4.4×10^{-5} M. The pattern expansion stops and after a few minutes, we are left with an irregular patch of clear spots (Figure 11b). The spots then slowly drift or dye to produce, after several hours, a stable and much more regular hexagonal array of spots (Figure 11c). The average distance between neighboring spots as a function of time is given in Figure 12. After the decrease in $[ClO_2]_0$, this

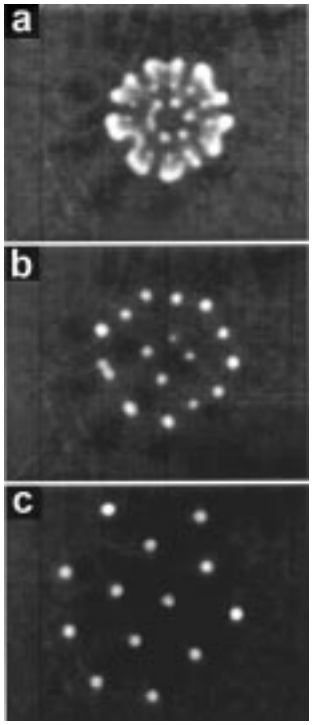

Figure 11. Localized patterned island. (a) Photograph taken just before $[ClO_2]_0$ is changed from 2×10^{-4} M to 0.49×10^{-4} M; (b) photograph taken 1 h after the change; (c) pattern obtained 17 h after the change. Experimental conditions $[MA]_0 = 7.8 \times 10^{-4}$ M, $[PVA]_0 = 4.5$ g/L, and all other parameters as in Figure 4.

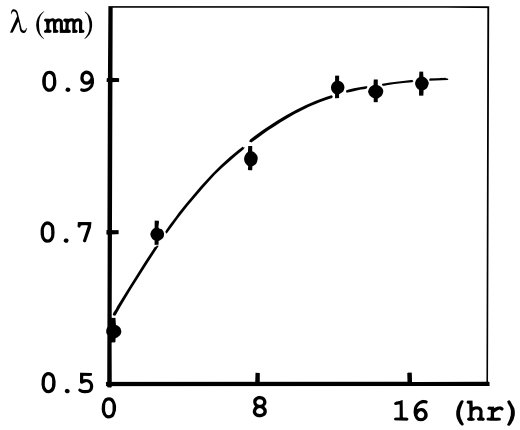

Figure 12. Average distance between first neighbor spots as a function of time in the localized pattern of Figure 11.

mean distance increases and stabilizes around 0.9 mm, a wavelength identical to that obtained when the Turing state tesselates the whole disk of gel (as reported in Table 2). If $[ClO_2]_0$ is increased to 6.7×10^{-5} M, the spots at the periphery of the cluster start to divide and the patterned Turing state ultimately fills the whole space. If conversely, $[ClO_2]_0$ is decreased to 3.9×10^{-5} M, such a small cluster slowly decays and a uniform state is obtained. The localization phenomenon observed is not linked to any inhomogeneity of the gel or in the feed process because different cluster sizes could be obtained for the same feed parameter values. The size of the cluster primarily depends on the stage of development of the flower-like pattern before its growth is quenched by decreasing $[ClO_2]_0$.

4. Discussion

The stability of moving interfaces between two states is a classic subject of study in many different fields which range

from directional solidification fronts in metal alloys, to viscous fingers in fluids, or to flames. Directional solidification fronts are accomplished in systems with moving driven temperature gradients. The front instability depends on many factors,[38] the most important of which are the diffusivity of impurities at the solidification front and the depletion exerted on the solidification temperature by the impurities and the curvature of the front. A great variety of frozen patterns are observed.[39] Viscous fingers are obtained by injecting a less viscous fluid into a more viscous immiscible fluid which occupies the gap between two plates.[40] They can produce more or less intricate patterns. In such systems, the complexity of pattern proceeds by a finger tip splitting mechanism. The size of fingers decreases with the increasing rate of injection of the less viscous fluid into the other. There is no characteristic wavelength in this process. In the case of flames, the stability of reaction−diffusion fronts has long been understood.[41] Flames are associated to reacting fronts between a state corresponding to a cold mixture of unburned-gas state and a hot burned-gas state. Planar flames can become spatially and temporally unstable if the stoichiometrically limiting reagent diffuses faster than the heat produced by the reaction, which activates the reaction. Different stationary and traveling front modulations can be obtained. The wavelength of these modulations is an intrinsic property of the reaction kinectics and of the diffusivity of species. However, flame fronts are often complicated by unavoidable fluid motions because of steep density changes between the initial and the final states.

Isothermal fronts between uniform states in autocatalytic systems have been known to exist for a long time.[42−44] As a result of a number of recent experimental developments, theoretical studies were reconsidered using formal kinetic models.[45] In two-variable systems, beside the necessary difference of diffusivity between an activatory and an inhibitory species, the destabilization of a planar front is only possible if there is at least a "cubic term" in the activatory chemical channel.[46] The nonplanar fronts develop a characteristic wavelength determined solely by the reaction kinetics and by the diffusion coefficients of species. In the moving frame of the wave, the transverse instability of a planar front bears many of the characteristics of the Turing instability; there are nonetheless important differences. Nonplanar wave fronts can develop in simple bistable systems wereas Turing patterns require kinetic mechanisms that support homogeneous oscillatory behavior. Recent theoretical approaches of front instabilities indicate that two main ingredients rule the nature and stability of transient and persistent patterns issued from front dynamics: (i) the nonequilibrium Ising/Bloch front transition,[47,48] that is, the transition from parameter regions where one or the other state always dominates to regions where either state can dominate depending on the initial conditions, and (ii) the transverse morphological instability of these two types of fronts.[44,48−50] Other recent theoretical studies analyze the consequences of the interaction between a Turing instability and a pitchfork bifurcation of uniform states.[51] This can modify the usual sequence of Turing planform bifurcation. In particular, the two inverted types of hexagon structures can become simultaneously stable. This type of coupling readily produces the following sequence of states: uniform state 1 ↔ hexagon 0 ↔ stripes ↔ hexagon π ↔ uniform state 2.

How does our observation relate to the different theoretical pictures mentioned above? One should first note that when a parameter jump is made directly from USS1 to USS2, a sharp front is obtained between USS1, which is now unstable, and USS2. The front between these two uniform states clearly undergoes a transverse morphological instability which manifests by the development of undulated propagating fronts, as illustrated in Figure 8. In this figure, one still witnesses transient striped Turing patterns, but for concentration jumps to still higher values of $[MA]_0$, only direct sharp transitions between the two uniform states are observed. This is one of the few examples of a propagating front instability in an isothermal chemical system. Morphological instabilities of traveling planar fronts had been previously reported in two clock reactions: the iodate−arseneous acid reaction in which iodide is the main activatory species,[52] and in the chlorite−tetrathionate reaction[53] in which the proton is the main activatory species.

Note that in the present case, the wavelength of the indentations of the front ranges between 1 and 2 Turing wavelengths. This implies a strong connection between this front instability and the Turing instability. All of the other pattern growth phenomena presented in this paper could be interpreted in the frame of an interaction between a propagating front linking two uniform states and a Turing instability. For $[PVA]_0$ as high as 10 g/L, the stirred tank composition shows no bistability between low and high potential stationary states; a rather smooth change of potential is observed as a function of $[MA]_0$. Nevertheless, we are led to suggest that, in phase space, the system evolves in the vicinity of a pleated slow manifold which stimulates the development of large amplitude Turing patterns. Note also that following the work of Métens et al.,[51] the observation of a transient inverted (black) hexagon pattern, at the high $[MA]_0$ limit of the Turing domain, could be an indication that the system operates in the close vicinity of pitchfork bifurcation of uniform states. During the pattern growth process, a front reminiscent of that linking USS1 and USS2 is thus transiently formed. While this front propagates into USS1, it excites the development of the stable Turing mode. When the concentration jump brings the system into the region of the stable striped Turing pattern (e.g., jump 3 in Figure 3), a smooth circular front between USS1- and USS2-type states develops and travels quite fast. For a critical low curvature, the uniformly curved front becomes transversally unstable and develops fingers which serve as "moving boundaries" for the unfolding of the striped Turing patterns which are layed in parallel to the fingers. As the fingers travel away from the center, the tip widens, then divides into two new daughter fingers as soon as the width of the tip is twice the Turing wavelength λ ($\lambda \sim 0.45$ mm). This infers that the finger splitting mechanism is connected to a morphological instability of the propagating front and that the selected wavelength is that of the stable Turing state.

For concentration jumps in the middle range of the Turing domain (e.g., jump 2 in Figure 3), the fingers still grow fast in the radial direction and thus excite elongated patterns. The development of the striped Turing mode is initially favored, but after some time many of these stripes break into spots. The spot mode dominates closer and closer to the front as the radial rate of expansion of the front decreases and as the final composition approaches the USS1 limit. For compositions sufficiently near those of USS1, the front travels very slowly and the Turing spot mode can develop simultaneously. It is the combination of these two factors that leads to the spot division mechanism described in this report. Note that, at least in the initial stages, the division proceeds alternatively in the radial and azimuthal directions. In the overall, the spot division and the tip splitting are dynamically very similar. As far as we know, no fingering process similar to the one reported here

had been previously reported for an isothermal reaction−diffusion system.

Spot divisions have already been observed both in experiments and in models.[11] They were first reported in experiments performed with the iodate−ferrocyanide−sulfite bistable reaction (EOE reaction).[10] Although such divisions bear strong similarities with those reported here (repulsion between neighboring spots and swelling of the spots in the direction of free space), several major differences should be noted. In the EOE reaction, an isolated spot swells to form an expanding annulus instead of dividing. Conversely, in the present experiments, for composition jumps close to USS1, an isolated spot spontaneously breaks the circular symmetry and divides when it reaches a critical size of the order of the Turing wavelength. This occurs whether it is initiated at a "dust particle" (as in Figure 3) or not. The other major difference is that in the present experiments, a stationary spot pattern is reached, whereas in the EOE reaction there is a continuous birth and death of spots and a stationary pattern never settles. Spot divisions leading to stationary hexagonal arrays of spots were previously reported in experiments with the CIMA reaction operated in a two-sided asymmetrically fed disk reactor.[8,28] In those experiments, it was not possible to correlate the "cell division" phenomenon to any dynamic specificity of the reaction, because of the strong parameter gradients and the unknown composition of the stratum where patterns develop. Here we are able to show that the spot division phenomenon goes together with a fingertip splitting phenomenon and all of this occurs in a region of contrasted Turing patterns enclosed between two different nearby uniform states.

The immobilization of front between two states can lead to localized states. Such a phenomenon of interface locking is well known in condensed matter physics in which it controls the dynamics of dislocations, charge density waves, or domain walls.[54] Discrete systems are prone to produce locked interfaces.[55] They have also been reported in continuum systems such in Benard−Marangoni convection cells in fluids.[56] In the domain of chemistry, the localization of a droplet of Turing state in an oscillatory state had been experimentally observed.[8] It was shown to lead to asymmetric quasi-one-dimensional wave sources or to different spiral-like wave phenomena in quasi-2-D oscillatory systems. These localization phenomena were shown to rely on both nonadiabatic and nonpotential effects because of the combination of oscillatory and periodic properties of the states involved. In the above-described experiments, no oscillatory instability is involved and one could think that the stabilization is primarily due to nonadiabatic effects linked to the periodic aspect of the Turing state, but isolated Turing spots can also readily be observed in this region of parameters so that nonpotential aspects must also play a major role. Although localized Turing states in a uniform state are well documented theoretically, the above observation is the first unambiguous experimental report on such an isolated pattern island clearly linked to a hysteresis phenomenon and not to small experimentally unavoidable spatial inhomogeneities of some control parameter.

5. Conclusion

We have described the propagation dynamics and different pattern mode selections of a pattern-forming state invading absolutely unstable uniform states. This was obtained by supercritical parameter jumps from initial uniform states into a domain of stable Turing patterns and by the introduction of a local spatial perturbation, in order to "nucleate" the patterned state. In addition to the classical mechanisms of pattern growth by addition of spot or band at the interface of the two states, we have also described two quite different but related pattern growth mechanisms: a spot division and a fingertip splitting process. The envelope of the front connecting the stable and unstable states moves at constant velocity. This velocity increases with the increasing size of the parameter jump. Within our experimental accuracy, the final wavelength of the patterns does not significantly depend on the history of the system, that is, on the way the asymptotic state was reached (large jump or smooth changes of parameter). However, the pattern dropped behind the front rearranges more or less rapidly and may even change planform. The global aspect of the pattern growth mechanism seems to depend on both the planform of the asymptotic stable state and on how close to the front the final pattern selection occurs.

Several theoretical works have considered such front propagations in "quenched" systems, with the aim of determining the rules of selection for the front velocity and for the pattern development.[57,58] The most striking results of these theoretical works are that the propagation velocity and the wavelength of the patterns are selected by marginal stability principle. In some cases, the wavelength of the pattern dropped behind a front can be significantly different from that obtained by a dense growth of the pattern out of the uniform state.[58] This was not observed in the present experiments, possibly because the wavelength of the patterns did not depend sensitively on the parameter ($[MA]_0$) used for the jumps. As for the marginal stability selection criteria, it is a very difficult property to establish experimentally, especially in quasi-2-D systems.

Moreover, the experimental situation described above was far more complex than that in the mentioned theoretical approaches. In the control parameter region explored, the Turing domain stands between two quite different uniform states and a transverse morphological instability of a front joining these two uniform states seems to come into play, in addition to the Turing instability. How much of this complexity really governs the pattern development reported is still not well established. Yet, here, we are inclined to think that the transverse morphological instability plays a key role. Our observations and the discovery of a growing variety of reaction−diffusion patterns call for a comprehensive study of the interaction between a Turing instability and a morphological instability of a propagating front. A number of universal aspects of front dynamics are reexamined by Hagberg and Meron[49] and, in many instances, these studies should be connected with those developed by Métens et al.[51,59] on the interaction of a Turing instability with a cusp bifurcation of uniform steady states.

On the other hand, experiments performed on modified versions of the CDIMA reaction tailored to produce bistability between uniform states in a CSTR are presently in progress with the aim to generate in widely separated regions of parameter: morphological instabilities of fronts linking these uniform states and a Turing instability. The ultimate goal is to study the new features emerging as these two instabilities are brought together. This is in principle possible, because the conditions for the development of morphological instabilities are less stringent than for the Turing instability, in particular concerning the necessary differences in diffusion coefficients of species.[59] From the practical point of view, a major difficulty in these studies will lay in the possible development of large subcritical branches of Turing patterns which may blur the difference, if any, between stationary patterns resulting from the folding of planar fronts or from highly contrasted patterns

in the continuation of a Turing branch. A large domain of hysteresis between a Turing state and a uniform state is already reported here and in this domain, a large variety of localized patterns could be obtained going from isolated spikes to sparse hexagonal arrays of spikes, depending on history of the system.

Acknowledgment. We thank J. Boissonade, P. Borckmans, G. Dewel, and S. Métens for stimulating discussions.

References and Notes

(1) Turing, A. M. *Philos. Trans. R. Soc. London, Ser. B* **1952**, *327*, 37−72.

(2) (a) Castets, V.; Dulos, E.; Boissonade, J.; De Kepper, P. *Phys. Rev. Lett.* **1990**, *64*, 2953−2956. (b) De Kepper, P.; Castets, V.; Dulos, E.; Boissonade, J. *Physica D* **1991**, *49*, 161−169.

(3) (a) Noszticzius, Z.; Horsthemke, W.; McCormick, W. D.; Swinney, H. L.; Tam, W. Y. *Nature* **1987**, *329*, 619. (b) Kreisberg, N.; McCormick, W. D.; Swinney, H. L. *J. Chem. Phys.* **1989**, *91*, 6532.

(4) (a) Boissonade, J.; Castets, V.; Dulos, E.; De Kepper, P. In *Bifurcation and Chaos: Analysis, Algorithms, Applications*; Seydel R., Schneider F. W., Küpper T., Troger H., Eds.; International Series of Numerical Mathematics 97; Birkhäuser: Basel, 1991; p 67. (b) Dulos, E.; Boissonade, J.; De Kepper, P. *Physica A* **1992**, *188*, 120.

(5) (a) Tam, W. Y.; Horsthemke, W.; Noszticzius, Z.; Swinney, H. L. *J. Phys. Chem.* **1988**, *88*, 3395. (b) Skinner, G.; Swinney, H. L. *Physica D* **1991**, *48*, 1.

(6) *ChemicalWaves and Patterns*; Kapral, R., Showalter, K., Eds.; *Understanding Chemical Reactivity 10*, Kluwer Academic Publisher: Dordrecht, 1994.

(7) Perraud, J. J.; De Wit, A.; Dulos, E.; De Kepper, P.; Dewel, G.; Borckmans, P. *Phys. Rev. Lett.* **1993**, *71*, 1272.

(8) De Kepper, P.; Perraud, J. J.; Rudovics, B.; Dulos, E. *Int. J. Bif. Chaos* **1994**, *4*, 1215−1231.

(9) (a) De Wit, A.; Dewel, G.; Borckmans, P. *Phys. Rev. E* **1993**, *48*, R4191−4194. (b) Lima, D.; De Wit, A.; Dewel, G.; Borckmans, P. *Phys. Rev. E* **1996**, *53*, R1−4.

(10) (a) Lee, K. J.; McCormick, W. D.; Ouyang, Q.; Swinney, H. L. *Science* **1993**, *261*, 192−194. (b) Lee, K. J.; Swinney, H. L. *Phys. Rev. E* **1995**, *57*, 1899−1915. (c) Lee, K. J.; Swinney, H. L. *Int. J. Bif. Chaos* **1997**, *7*, 1149−1158.

(11) Pearson J. E. *Science* **1993**, *261*, 189−191.

(12) (a) Zaikin, A. N.; Zhabotinsky, A. M. *Nature* **1970**, *225*, 535. (b) Zhabotinsky, A. M.; Zaikin, A. N. *J. Theor. Biol.* **1973**, *40*, 45.

(13) Zykov, V. S. Simulation of wave processes in excitable media. In *Nonlinear Science Theory and Application*; Manchester University Press: Manchester, 1987.

(14) Meinhardt, H. *Models of Biological Patterns Formation*; Academic Press: London, 1982.

(15) Babloyantz, A. *Molecules, Dynamics and Life*; Wiley: New York, 1986.

(16) Murray, J. D. *Mathematical Biology*; Spinger: Berlin, 1989.

(17) Harrison, L. G. *Kinetic Theory of Living Patterns*; Cambridge University Press: New York, 1993.

(18) Nicolis, G.; Prigogine, I. *Self-Organization in Nonequilibrium Chemical Systems*; Wiley: New York, 1977.

(19) (a) Ouyang, Q.; Swinney, H. L. *Nature* **1991**, *352*, 610. (b) Ouyang, Q.; Noszticzius, Z.; Swinney, H. L. *J. Phys. Chem.* **1992**, *96*, 6773−6776.

(20) Lengyel, I.; Kadar, S.; Epstein, I. R. *Science* **1993**, *259*, 493−495.

(21) De Kepper, P.; Epstein, I. R.; Kustin, K.; Orbán, M. *J. Phys. Chem.* **1982**, *86*, 170.

(22) Lengyel, I.; Rabai, G.; Epstein, I. R. *J. Am. Chem. Soc.* **1990**, *112*, 4606; **1990**, *112*, 9104.

(23) Ouyang, Q.; Gunaratne, G. H.; Swinney, H. L. *Chaos* **1993**, *3*, 707.

(24) Ouyang, Q.; Swinney, H. L. *Chaos* **1991**, *1*, 411.

(25) Dulos, E.; Davies, P.; Rudovics, B.; De Kepper, P. *Physica D* **1996**, *98*, 53−66.

(26) Rudovics, B.; Dulos, E.; De Kepper, P. *Phys. Scripta* **1996**, *T67*, 43−50.

(27) Lengyel, I.; Epstein, I. R. *Science* **1990**, *251*, 650−652; *Proc. Natl. Acad. Sci. U.S.A.* **1992**, *89*, 3977−3979.

(28) Rudovics, B. Ph.D. Thesis, No. 1358, University Bordeaux I, 1995.

(29) Barillot, E. Ph.D. Thesis, No. 1567, University Bordeaux I, 1996.

(30) Rudovics, B.; Barillot, E.; Davies, P. W.; Dulos, E.; Boissonade, J.; De Kepper, P. Submitted for publication to *J. Phys. Chem.*, 1998.

(31) Chlorine dioxide is produced by acidic oxidation of sodium chlorite by sodium persulfate. The gaseous product is exacted from the liquor by air bubbling and redissolved in an ice-cold solution of 1 M sulfuric acid (this method was initially proposed by I. Nagypal, private communication). The chlorine dioxide solutions are titrated by a standard iodometric volumetric method.

(32) Volford, A.; Wittman, M.; Marlovits, G.; Noszticzius, Z. *J. Phys. Chem.* **1997**, *101*, 3720−3726.

(33) Lengyel, I.; Li, J.; Kustin, K.; Epstein, I. R. *J. Am. Chem. Soc.* **1996**, *118*, 3708−3719.

(34) Ouyang, Q.; Li, R.; Li, G.; Swinney, H. L. *J. Phys. Chem.* **1995**, *102*, 2251−2555.

(35) (a) Jensen, O.; Pannbaker, V. O.; Dewel, G.; Borckmans, P. *Phys. Lett.* **1993**, *A179*, 91−96. (b) Jensen, O.; Pannbaker, V. O.; Mosekilde, E.; Dewel, G.; Borckmans, P. *Phys. Rev. E* **1994**, *50*, 736−749.

(36) Pomeau, Y. *Physica D* **1986**, *23*, 3−11.

(37) Thual, O.; Fauve, S. *J. Phys. (Paris)* **1988**, *49*, 1829−1833.

(38) Flesselles, J.-M.; Simon, A. J.; Libchaber, A. J. *Adv. Phys.* **1991**, *40*, 1−51.

(39) Oswald, P.; Melo, F. In *Growth and Form: Nonlinear Aspects*; Ben Amar, M., Pelcé, P., Tabeling, P., Eds.; NATO ASI Series 276, Plenum Press: New York, London, 1991; pp 177−185.

(40) Arnéodo, A.; Argoul, F.; Couder, Y.; Rabaud, M. In *Growth and Form: Nonlinear Aspects*; Ben Amar, M., Pelcé, P., Tabeling, P., Eds.; NATO ASI Series 276, Plenum Press: New York, London, 1991; pp 287−327.

(41) Sivashinsky, G. I. *Annu. Rev. Fluid Mech.* **1991**, *15*, 241.

(42) (a) Luther, R. *Z. Electrochem.* **1906**, *12*, 596. (b) Gray, P.; Sholwalter, K.; Scott, S. K. *J. Chim. Physique* **1987**, *84*, 1329−1333.

(43) Ortoleva, P.; Ross, J. *J. Chem. Phys.* **1974**, *60*, 5090; **1975**, *63*, 3398.

(44) Kuramoto, Y. *Chemical Oscillations, Waves and Turbulence*; Springer Series in Synergetics 19, Springer-Verlag: Berlin, 1984.

(45) Scott, S. K.; Showalter, K. *J. Phys. Chem.* **1992**, *96*, 8702.

(46) Horváth, D.; Petrov, V.; Scott, S. K.; Showalter, K. *J. Phys. Chem.* **1993**, *98*, 6332−6343.

(47) Coullet, P.; Lega, J.; Houchmanzadeh, B.; Lajzerowicz, J. *Phys. Rev. Lett.* **1990**, *65*, 1352. Coullet, P.; Lega, J. *Europhys. Lett.* **1988**, *7*, 511.

(48) Ohta, T.; Mimura, M.; Kobayashi, R. *Physica D* **1989**, *34*, 115.

(49) (a) Hagberg, A.; Meron, E. *Phys. Rev.* **1993**, *48*, 705−708. (b) Hagberg, A.; Meron, E. *Nonlinearity* **1994**, *7*, 805−835. (c) Hagberg, A.; Meron, E. *Chaos* **1994**, *4*, 477−484. (d) Hagberg, A.; Meron, E.; Rubinstein, I.; Zaltman, B. *Phys. Rev. E* **1997**, *55*, 4450−4457.

(50) Petrich, D. M.; Goldstein, R. E. *Phys. Rev. Lett.* **1994**, *72*, 1120−1123.

(51) Métens, S.; Dewel, G.; Borckmans, P.; Engelhardt, R. *Europhys. Lett.* **1997**, *37*, 109−114.

(52) Horváth, D.; Showalter, K. *J. Chem. Phys.* **1995**, *102*, 2471−2478.

(53) (a) Tóth, A.; Lagzi, I.; Horváth, D. *J. Phys. Chem.* **1996**, *100*, 14837−1439. (b) Horváth, D.; Tóth, A. *J. Chem. Phys.* **1998**, *108*, 1447−1451.

(54) Peyrard, M.; Kruskal, M. D. *Physica D* **1984**, *14*, 88.

(55) (a) Laplante, J. P.; Erneux, T. *Physica A* **1992**, *188*, 89. (b) Willebrand, H.; Radehaus, C.; Niedernostheide, F-J.; Dohmen, R.; Purwins, H.-G. *Phys. Lett.* **1990**, *A149*, 131.

(56) Bensimon, D.; Shraiman, B. I.; Croquette, V. *Phys. Rev. A* **1988**, *38*, 5461.

(57) (a) Ben-Jacob, E.; Brand, H.; Dee, G.; Kramer, L.; Langer, J. S. *Physica D* **1985**, *14*, 348−364. (b) Dee, G. *J. Stat. Phys.* **1985**, *39*, 705−717.

(58) Jensen, O.; Pannbacker, V. O.; Mosekilde, E.; Dewel, G.; Borckmans, P. *Phys. Rev. E* **1994**, *50*, 736−747.

(59) Métens, S. Ph.D. Thesis, Université Libre de Bruxelles, March 1998.